Optical coherence techniques for plasma spectroscopy (invited)

J. Howard,[a] C. Michael, F. Glass, and A. D. Cheetham
Plasma Research Laboratory, Australian National University, Canberra ACT 0200, Australia

(Presented on 21 June 2000)

A new electro-optically modulated optical solid-state (MOSS) spectrometer has been constructed for high temporal resolution measurement of the coherence of line radiation from plasmas. The instrument is an electro-optically modulated fixed delay polarization interferometer, or Fourier transform spectrometer. It has high light throughput compared with conventional grating based instruments of comparable resolving power while being compact and robust against alignment errors. By employing electro-optical path-length modulation techniques, the spectral information is transferred to the temporal frequency domain and can be obtained using a single photodetector. A wide field-of-view MOSS camera has been developed for imaging applications, while multiple-delay variants of the basic single fixed delay instrument have also been successfully tested. We discuss applications including passive Doppler spectroscopy, charge exchange recombination spectroscopy, and Zeeman and motional Stark effects. For Doppler tomographic applications, we show that such time-domain instruments have certain fundamental advantages, not least of which is a simple relationship between fringe visibility and the line integral of the intensity weighted velocity distribution function. © *2001 American Institute of Physics.* [DOI: 10.1063/1.1326901]

I. INTRODUCTION

This article describes an electro-optically modulated solid state (MOSS) spectrometer for general purpose optical plasma spectroscopy.[1,2] The spectrometer monitors the temporal coherence of an isolated spectral line using polarization interferometric techniques. It is essentially a Fourier transform spectrometer (FTS) modulated about a fixed delay. The amplitude of the interference fringes produced by the modulation is related to the light temporal coherence while the phase conveys the line center frequency.

It is well known that the FTS can provide a significant light throughput advantage over an equivalent resolution grating based instrument.[3] However, this is often offset by the necessity to mechanically scan the optical path length delay in order to reconstruct the spectrum. The interferometric nature of the instrument also requires a high degree of mechanical stability. Fixed systems based on polarizing optics which form the interferogram in the spatial domain[4] overcome many of these problems, but again require the light to be dispersed and received by many detectors in order that the spectrum can be reconstructed. However, when the spectrum can be simply parametrized (for example, in terms of its intensity, shift, and width), measurements at a single, or perhaps only a few delays simultaneously may suffice for its characterization. This allows the photon flux to be divided among a small number of detectors.

It is a remarkable fact that, notwithstanding the complications owing to integration over an inhomogeneous source, measurements at a fixed (but temporally modulated) delay are sufficient for tomographic reconstruction of the intensity, flow, and temperature fields for Doppler broadened emission lines. This allows high time resolution to be obtained (only a single detector is required) and opens the possibility for two-dimensional spectroscopic imaging using a camera and two-dimensional multianode photomultipler tube detector (MAD) array.

In this article we discuss a number of experiments based on MOSS technology that are presently installed on the H-1 heliac at the Australian National University.[5] These include a fixed and moveable single channel systems, the MOSS spectroscopic camera,[6] the tomographic MOSS (ToMOSS) spectroscopy system,[7] and the spread-spectrum optical Fourier transform (SOFT) spectrometer.

In Sec. I we introduce the MOSS hardware and review the measurement principle. It is shown that, for a plasma in local thermal equilibrium, a single delay MOSS system delivers well-defined information about the line-integrated temperature distribution. To tomographically unfold this requires simultaneous measurements at many positions and many angles. To this end we have developed a wide field-of-view MOSS camera that registers a discretized projection of the H-1 poloidal plasma cross section using a linear MAD array. The projection can be Abel inverted to obtain time resolved images of the plasma emission intensity, temperature, and flow vorticity (Sec. III). For higher resolution studies, we have constructed the ToMOSS system, a rotatable apparatus that encircles the H-1 plasma and supports five arrays of 11 lens-coupled optical fibers. All 55 optical fibers are imaged through a single MOSS camera onto an 8×8 MAD array.

The SOFT system (Sec. IV) is an extension of the MOSS concept to simultaneous coherence measurements at multiple fixed delays. Such a system is required when more detailed line shape information is required (for example, to study nonthermal distributions). Under certain conditions, it is possible to reconstruct the velocity distribution function of the emitting species.[8]

[a]Author to whom correspondence should be addressed; electronic mail: john.howard@anu.edu.au

 © 2001 American Institute of Physics

Downloaded 20 Jun 2001 to 150.203.2.85. Redistribution subject to AIP license or copyright, see http://ojps.aip.org/rsio/rsicr.jsp

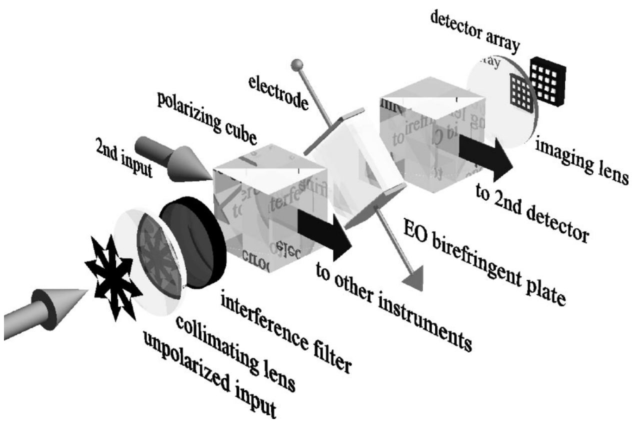

FIG. 1. Optical layout for the modulated solid state spectrometer.

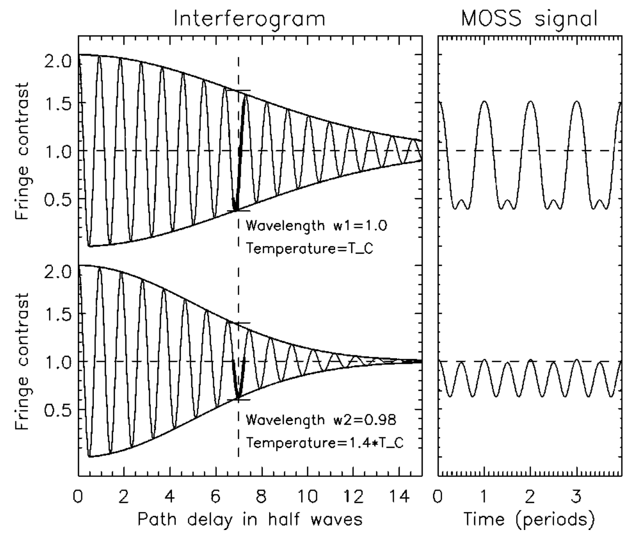

FIG. 2. Simulated interferograms showing the effect on the interferogram phase of a change in line center frequency (exaggerated for clarity). The dashed vertical line corresponds to the delay introduced by the birefringent crystal while the bold section is the portion of the interferogram swept by the electro-optic modulation. The fringe contrast also varies with changes in the temperature of the emitting species. The temporal signal resulting from the modulation is shown on the right.

Finally, we consider some important potential applications in polarization spectroscopy such as motional Stark effect and Zeeman spectroscopy. As we show in Sec. VI, MOSS-based systems for such measurements offer simplifications in optical design and improvements in measurement signal to noise ratio.

II. STATIC FOURIER TRANSFORM SPECTROSCOPY

The MOSS spectrometer is an electro-optically modulated, fixed delay FTS based on solid polarizing optical components. Its behavior can be understood in terms of standard theory for Fourier transform spectrometers.[9] We represent by $e(\xi)$ the species emission line spectrum, where $\xi=(\nu-\nu_0)/\nu_0$ is the normalized frequency and ν_0 is the line center frequency in the particle rest frame. The signal obtained using an ideal FTS can be expressed as

$$S_\pm(\phi)=\frac{\mu_0}{2}[1\pm\mathscr{R}[\gamma(\phi)\exp(i\phi)]], \tag{1}$$

where μ_0 is the line integrated emission intensity, $\phi=2\pi\nu_0\tau$, where τ is the interferometer time delay and $\gamma(\phi)$ is the optical coherence, related to the light spectral distribution through the Weiner–Khinchine theorem

$$\gamma(\phi)=\frac{1}{\mu_0}\int_{-\infty}^{\infty}e(\xi)\exp(i\phi\xi)d\xi. \tag{2}$$

In conventional FTS, the path length is mechanically scanned and the recorded interferogram is inverted for the spectrum $e(\xi)$. For high-resolution plasma spectroscopy applications, it is often sufficient to fix the delay and temporally monitor variations in the light coherence.

The layout of the MOSS spectrometer is shown in Fig. 1. A narrow band interference filter isolates the spectral line of interest. The first polarizing cube transmits the horizontally polarized component of the filtered plasma light to a birefringent crystal (typically $LiNbO_3$, $L=25$ mm thick, birefringence $B=0.1$) whose fast axis is at 45° to the plane of polarization. For light of center frequency ν_0, this introduces a fixed phase delay $\phi_0=2\pi\nu_0BL/c=2\pi\nu_0\tau_0$ between the orthogonal characteristic waves. The light is finally polarized using a beamsplitter cube to allow the independent components to interfere at photomultiplier tubes intercepting the transmitted and/or reflected beams.

The operating principle is illustrated in Fig. 2. When the species temperature increases (decreases), the fringe visibility $|\gamma(\phi)|$ decreases (increases). This is monitored by dithering the instrument phase electro-optically by an amount $\tilde{\phi}_1=\phi_1\cos(\Omega t)$ of amplitude $\phi_1\gtrsim\pi/2$ about the fixed delay (phase) offset ϕ_0. The modulation is imposed by applying an oscillating voltage (typically at tens of kilohertz) along the crystal z axis. When the center frequency changes, the interferogram expands or contracts leaving the envelope unchanged. This is registered as a change in the ratio of the power in the odd and even harmonics of the applied modulation. Because of the large fixed delay τ_0, even small changes in wavelength can give significant shifts in the interferogram phase.

We write for the instantaneous phase shift

$$\phi=\phi_0+\phi_1\cos\Omega t \tag{3}$$

so that the available information bandwidth is determined by the modulation angular frequency Ω. Substituting from Eq. (3) in Eq. (1), and applying simple trigonometric identities yields

$$S_\pm(\phi)=\mu_0[1\pm\gamma_c\cos(\phi_1\cos\Omega t)\mp\gamma_q\cos(\phi_1\cos\Omega t)], \tag{4}$$

where $\gamma=\gamma_c+i\gamma_q=|\gamma|\exp(i\phi_0)$. Using the Bessel expansion, it can be shown that even and odd harmonics of the modulation frequency are proportional, respectively, to γ_c and γ_q.

Downloaded 20 Jun 2001 to 150.203.2.85. Redistribution subject to AIP license or copyright, see http://ojps.aip.org/rsio/rsicr.jsp

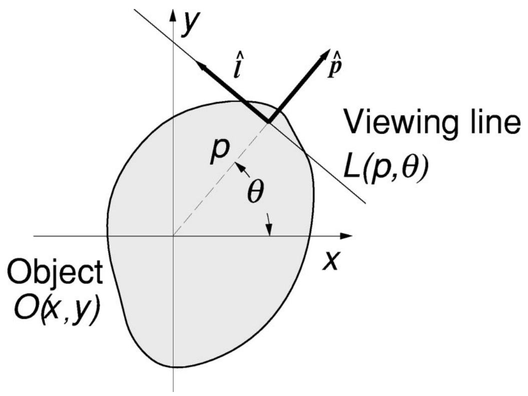

FIG. 3. Geometry for tomography of some $2d$ scalar function O showing relationship between unit vector $\hat{\mathbf{l}}$ and the viewing line $L(p,\theta)$ at impact parameter p and angle θ.

The most basic optical spectroscopy measures the Doppler shift and broadening of emission from excited plasma atoms and ions. Though charge exchange recombination spectroscopy achieves a degree of localization, line integration effects can not generally be ignored. Multichannel measurements and tomographic techniques must then be employed. However, because of the summation of Doppler spectra of varying width and shift along the line-of-sight, spectral-domain (i.e., grating based) systems are not well suited for the inverse procedure.

The measured emission spectrum $e(\xi;\mathbf{l})$ depends on ξ and the direction of view $\mathbf{l}=p(-\sin\theta,\cos\theta)$, where p is the impact parameter and θ is the angle of the viewing line (see Fig. 3). On the other hand, the velocity distribution is a function of four coordinates $f=f(x,y,v_x,v_y)$. When the distribution is isotropic, however, we have $f=f(x,y,v)$ and the inverse problem is, in principle, no longer singular.

For an inhomogeneous drifting isotropic velocity distribution function $f(\mathbf{r},\mathbf{v}-\mathbf{v}_D)\equiv f_0(\mathbf{r},v)$, where $\mathbf{v}=\mathbf{V}/c$ is a normalized velocity coordinate, $v=|\mathbf{v}|$ and $\mathbf{v}_D(\mathbf{r})$ is the local first moment drift velocity, the integrated measurement along the line L viewing the plasma in direction $\hat{\mathbf{l}}$ is proportional to

$$e(\xi;\mathbf{l})=\int_L g(\mathbf{r},\xi;\hat{\mathbf{l}})\,dl, \tag{5}$$

where

$$g(\mathbf{r},\xi;\hat{\mathbf{l}})=\int f(\mathbf{r},\mathbf{v}-\mathbf{v}_D)\,\delta(\xi-\mathbf{v}\cdot\hat{\mathbf{l}})\,d\mathbf{v} \tag{6}$$

is the local emission spectrum with spectrally integrated isotropic intensity

$$I_0(\mathbf{r})=\int g(\mathbf{r},\xi;\hat{\mathbf{l}})\,d\xi. \tag{7}$$

The delta function selects the part of the velocity distribution f that contributes via the Doppler effect to the optical intensity at normalized frequency ξ.

Note that the Fourier transform of Eq. (6) over the normalized frequency coordinate separates the contributions from the drift and the body of the distribution

$$G(\mathbf{r},\phi\hat{\mathbf{l}})\equiv\mathscr{F}[g(\mathbf{r},\xi;\hat{\mathbf{l}})]=\exp(i\phi\mathbf{v}_D\cdot\hat{\mathbf{l}})G_0(\mathbf{r},\phi). \tag{8}$$

$G_0(\mathbf{r},\phi)$ gives a central slice of the Fourier transform of the spherically symmetric (isotropic) distribution $f_0(\mathbf{r},v)$. Combining Eqs. (2) and (5), and assuming conditions of local thermodynamic equilibrium (LTE), the fringe visibility assumes the particularly simple form[8]

$$|\gamma(\phi;\mathbf{l})|=\frac{1}{\mu_0}\int_L I_0(\mathbf{r})\exp[-T_S(\mathbf{r})/T_C]\,dl, \tag{9}$$

where $T_S(\mathbf{r})$ is the local species temperature. T_C is a ''characteristic temperature'' set by the total interferometer phase delay ϕ:

$$kT_C=\frac{1}{2}m_S V_C^2 \quad V_C=\frac{2c}{\phi}, \tag{10}$$

where $v_C=V_C/c$ is the corresponding ''characteristic velocity.'' (Note that, in calculating T_C, it is important to take account of the variation of the crystal birefringence with wavelength.) Observe that the fringe visibility is independent of the spatially varying drift $\mathbf{v}_D$ and can be inverted for the isotropic but inhomogeneous distribution function $f_0(\mathbf{r},v)$.[8]

The change in the interferometer phase due to the Doppler shift is given (to first order in small quantities) by

$$\frac{\delta\phi}{\phi}=\frac{1}{\mu_0|\gamma|}\int_L G_0(\mathbf{r},\phi)\mathbf{v}_D\cdot d\mathbf{l}, \tag{11}$$

where $d\mathbf{l}\equiv\hat{\mathbf{l}}dl$. Note that the usually small Doppler shift component $\delta\phi$ is magnified by the approximately constant fixed phase delay $\phi=\phi_0$. Equation (11) is a vector field line integral whose inversion gives the vorticity of the field $G_0\mathbf{v}_D$. Under appropriate conditions, it is possible to reconstruct the component of the flow-field vector potential that is normal to the measurement plane.[10]

Because frequency domain spectrometers resolve the line shape, all wavelength components are required to be measured in order to estimate the line-averaged distribution function parameters. This requires temporal path-length scanning in the case of a Fabry–Pérot, or a multichannel detector array for grating-based instruments. The coherence at a fixed delay, however, registers simultaneously contributions from all frequency components without the loss of light attending the need for spectral discrimination, namely high instrument finesse or a narrow input slit. Moreover, when the distribution function can be simply parametrized, the measured fringe visibility and phase relate directly to line integrals of these parameters. The MOSS spectrometer is therefore optimum for Doppler tomography in the sense that all of the photons available determine only the three independent pieces of information carried at dc and odd and even harmonics of Ω, namely μ_0, γ_c, and γ_q. These in turn are linked via line integrals to the unknown velocity distribution parameters I_0, T_S, and $\mathbf{v}_D$, which can then be recovered by tomography.

III. SINGLE CHANNEL MOSS SPECTROMETER

The MOSS optical components are mounted inside modular, flanged light-tight housings that allow flexible as-

Downloaded 20 Jun 2001 to 150.203.2.85. Redistribution subject to AIP license or copyright, see http://ojps.aip.org/rsio/rsicr.jsp

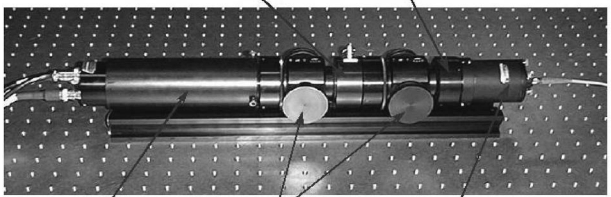

FIG. 4. Photograph of MOSS spectrometer with major components labeled.

sembly. The system is robust against minor optical misalignments. A small number of $LiNbO_3$ crystals of assorted lengths can be combined to obtain a characteristic temperature T_C (delay) that best matches the expected species temperature T_S. In our experiments, light is coupled into the MOSS using a lens-coupled optical fiber (numerical aperture $=0.4$) that approximately collimates the light through the birefringent components. Photomultiplier tubes, often mounted at both output polarizing cube ports, intercept the expanded light beam. Where possible, optical components are broadband antireflection coated. By mounting the interference filter directly in front of the photomultiplier tube, emission from different spectral lines can be monitored simultaneously at each of the final polarizer ports. Alternatively, the filter can be mounted at the fiber input, the use of two detectors then bringing a $\sqrt{2}$ improvement in signal to noise ratio. Figure 4 shows a photograph of a simple modular MOSS system.

We have made measurements for a number of atomic and ionic transitions in argon and helium discharges in the H-1 heliac. Light from a laser source (in our case, 488 nm) or standard lamp, suitably attenuated to match the plasma light intensity and temporally gated so as not to coincide with the plasma pulse, can be admitted through the unused input port of the first polarizing cube. This light signal allows us to compare the level of photon shot noise with the natural plasma light fluctuation level.

The high voltage modulation of the electro-optic plate(s) is achieved using a function generator, a standard audio amplifier, and step-up transformer (100:1). This system has been optimized using a detailed circuit model and is capable of operating over a range of frequencies from 0.5 to 100 kHz. For modulation frequencies in the range 0–20 kHz, the low level signal to the modulator is provided by a PC card (PCI-MIO-16E-4) controlled using a LabVIEW virtual instrument. The card/software also acquires the MOSS signals, processes, displays, and archives the data from up to eight channels in real time. For the results reported here (obtained at 30–40 kHz), we have synchronously ($n\Omega/2\pi$) acquired the data using CAMAC hardware and demodulated the interferograms numerically.

If we ignore the spatial integration and assume LTE, Eq. (1) gives the signal at the spectrometer ports as

$$S_{\pm}=I_0\pm I_0\zeta\cos[\phi_0(1+v_D)+\phi_1\cos(\Omega t)], \tag{12}$$

where the total fringe visibility $\zeta=\zeta_I\zeta_S$ now includes an instrumental component ζ_I analogous to the familiar slit function for grating spectrometers and $\zeta_S\equiv|\gamma|=\exp(-T_S/T_C)$, where T_S is the source temperature. The phase includes the Doppler shift $v_D=\delta\phi/\phi_0$ given by Eq. (11). The instrumental fringe contrast ζ_I is determined by the collected light solid angle and optical imperfections, and can be represented by the factor $\zeta_I=\exp(-T_I/T_C)$, where T_I is the instrument ''temperature.'' It is apparent that the source temperature T_S can be obtained from the measured fringe contrast via a simple subtraction of exponents proportional to the measured and instrumental temperatures rather than requiring the usual deconvolution correction for the instrument function.

Uncertainty in the instrumental phase offset ϕ_0 is equivalent to a wavelength calibration error for grating instruments. Because of thermal drifts and uncertainties in the numerical values of the refractive indices, it is difficult to absolutely determine the phase shift ϕ_0. Estimates of the Doppler drift v_D are usually obtained with respect to the measured phase ϕ_0 at the commencement of the discharge.

The H-1 heliac is a toroidal magnetic plasma confinement device having major radius $R=1$ m and average minor radius $a\sim0.2$ m. For the experiments reported here, the magnetic field strength on axis was varied between 0.1 and 0.3 T, while the magnetic configuration could be changed by independently controlling the currents flowing in the vertical field coils and the toroidal and poloidal coil sets. To demonstrate the spectrometer performance, we show temperature and flow data for radio frequency (rf) heated (7 MHz, 80 kW max) argon discharges.

Ar II light at 488 nm is collected from a cylindrical plasma volume of diameter ~30 mm that views the plasma toroidally. Fixed and translatable lens-coupled optical fibers that collect the light from other positions are also available. Almost complete poloidal cross-sectional data are obtained using the MOSS camera (Sec. IV). MOSS has been used for basic plasma ion-temperature scaling studies as well as for for study of ion dynamics during confinement transitions and during power modulation experiments. By virtue of its high light throughput (in our case, more than 3 orders of magnitude greater than for an equivalent-resolution grating instrument) the MOSS spectrometer is also especially well suited to measurements that require high time resolution such as for the observation of fluctuations and coherent modes.

The argon ion temperatures are in the range 10–100 eV and match well the dynamic range for a $LiNbO_3$ crystal of thickness 40 mm ($T_C=28$ eV) obtained by combining separate plates of thickness 15 and 25 mm. The instrument contrast, measured using an expanded argon ion laser beam at 488 nm, is typically 0.75 and arises mainly from imperfections in the birefringent plate. A more comprehensive discussion of instrument function, light throughput, resolution and noise sensitivity, and calibration procedures can be found elsewhere.[2]

To illustrate the MOSS performance we show data for a low field (~0.14 T) argon discharge that collapses to an unstable oscillation about 10 ms into the pulse. Figure 5 shows data obtained using a toroidally viewing single chan-

Downloaded 20 Jun 2001 to 150.203.2.85. Redistribution subject to AIP license or copyright, see http://ojps.aip.org/rsio/rsicr.jsp

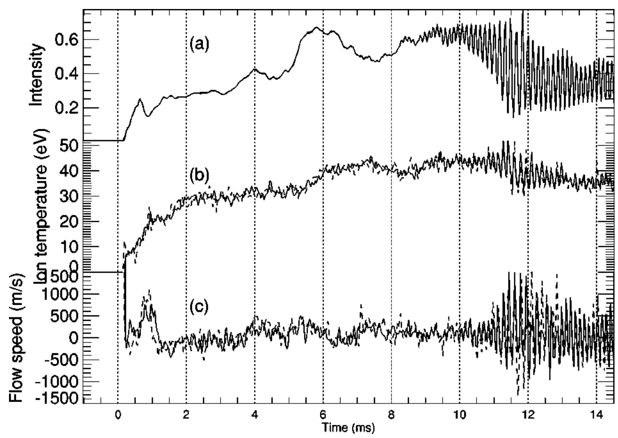

FIG. 5. (a) Light intensity at 488 nm (b) toroidal temperature and (c) the toroidal flow velocity. See text for discussion.

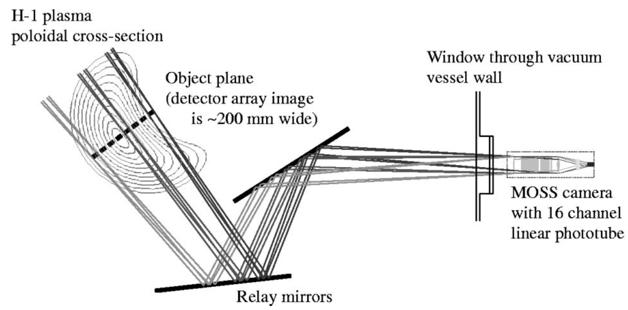

FIG. 6. Scale drawing showing the camera viewing geometry.

nel MOSS spectrometer. Signals (a)–(c) are the inferred intensity, ion temperature, and flow. In this figure we have superimposed the signals extracted independently from the interferograms at the transmit and reflect ports of the final polarizer. The noisier signal was monitoring the ''dark'' half of the interference fringe. Note the temporal resolution of both temperature and flow velocity oscillations. For comparison, trace (d) shows the line integrated plasma density measured using the scanning far infrared (FIR) interferometer.[11] Each trace in (d) represents a spatial sweep of the 743 μm laser beam over a partial plasma cross section.

IV. TOMOGRAPHIC SYSTEMS—THE MOSS CAMERA

Using imaging optics, it is possible to construct a multichannel MOSS camera. Rays from different plasma spatial positions are angularly multiplexed through the MOSS optical components. Because of the temporal encoding of the spectral information, the camera is a truly two-dimensional time-resolved imaging spectrometer. Each spatial channel requires its own detector, and the associated signals must be separately amplified and acquired. Commercially available multianode photomultiplier detectors are well suited for this application.

We have constructed two cameras. One directly images the poloidal plasma cross section onto a 16 element linear detector array.[6] The second camera utilizes an 8×8 MAD array to process light from an array of 55 intravacuum lens-coupled optical fibers.[7] The MOSS camera uses standard photographic lenses and 50 mm optics with typically ~40 mm clear aperture to match that of the birefringent plates. The camera is also modular in construction, the various flanged components are butted together and bolted to an optical rail. Details of the camera optical construction and its calibration are given elsewhere in these proceedings.[6]

The MOSS camera is mounted in front of a vacuum tank port and views the plasma via a pair of elongated flat mirrors that are supported inside the vacuum tank. The viewing geometry for the camera is shown in Fig. 6. Channel zero corresponds to the chord closest to the poloidal ring conductor. The full angle subtended by the plasma at the detector plane is ~6.5° while the imaging system magnification is 10×–15×. We have not yet attempted to tomographically unfold the data presented here.

Loss of instrument contrast associated with the angular variation of the refractive index of the lithium niobate birefringent plate limits the camera field-of-view to approximately 3° full cone angle for 50% contrast degradation. For given field-of-view and ionic species, the degradation varies as $1/T_C$ (lower temperature means greater coherence and longer path delay). The effect is analogous to the appearance of circular fringes in a Michelson interferometer for off-axis rays. This limitation would significantly compromise the camera light gathering power. Fortunately, a simple field-widening strategy where the single birefringent plate is replaced by twin crossed birefringent plates with an intervening half wave plate at azimuth 45° can be used to compensate this effect.[12] The resulting field-of-view is expanded by a factor $[2\sqrt{2}n/B]^{1/2}\sim 8$, eliminating this problem for the H-1 camera. Of more importance in the wide angle limit is the variation in the passband of the interference filter and possible light loss due to vignetting. Apart from the use of a suitable imaging system and the field-widening half-wave plate, the camera construction and operation is similar in other respects to the single-channel instrument. The instrument contrast and interchannel relative phase shifts are measured by illuminating the field-of-view with a suitably diffused light source (in our case, the laser beam) having a wavelength at or near the wavelength of interest. Additional instrumental details can be found in an accompanying article.[6]

A. Results

The camera reveals a more complete picture of the dynamics of the unstable discharge shown in Fig. 5. The time-resolved projections of light intensity, temperature, and flow are presented in Figs. 7 and 8. In the first, a 1.0 ms running mean has been applied to the signals to suppress the oscillating components. The plasma ion temperature profile is distinctly hollow (though the pressure profile is peaked) while the ''mean'' temperature appears to be consistent with that measured in the toroidal direction (intensity weighting must be considered for a true comparison). The hollow temperature profiles have been confirmed using a single channel MOSS and shot-to-shot measurements. When interpreting these results, it must be borne in mind that the magnetic axis intersects the vertical measurement plane at ≈30° so that

Downloaded 20 Jun 2001 to 150.203.2.85. Redistribution subject to AIP license or copyright, see http://ojps.aip.org/rsio/rsicr.jsp

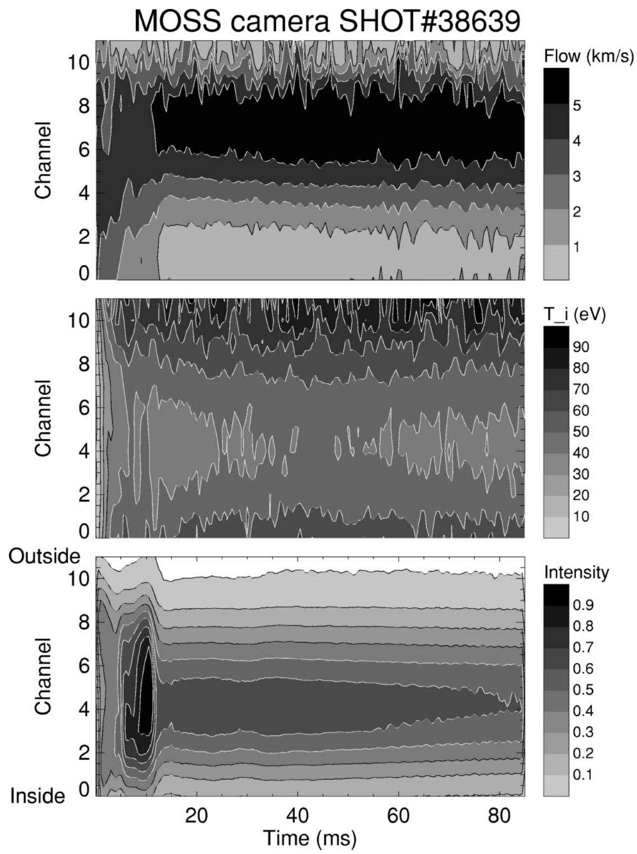

FIG. 7. Smoothed projections of the 488 nm emission intensity, temperature, and flow speed for a low field argon discharge. Channel 0 views the inside edge of the plasma, channel 11, the outside. See the text for discussion.

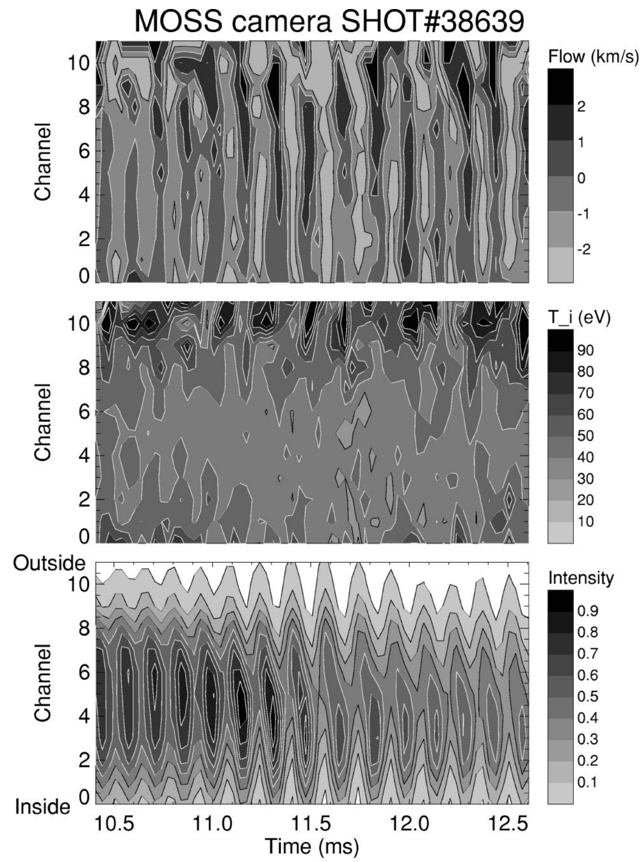

FIG. 8. Expanded view of camera projection data showing growth of the instability and ensuing plasma collapse. See the text for discussion.

both toroidal and poloidal behaviors are sensed by the measurements.

A number of mechanisms have been proposed for the high ion temperatures observed in H-1. The elevated temperature in the plasma edge may be evidence for direct particle acceleration in the rf sheath—an effect that may be important when the ion transit time through the sheath is on the order of the rf period.[13] The thermal speed for 50 eV argon ions is $v_{\mathrm{th}}=(2kT/m_S)^{1/2}\sim 1.5\times 10^4$ m/s and the Larmor radius is about 0.05 m, a sizable fraction of the mean plasma radius $a \lesssim 0.25$ m. Under such circumstances, direct ion orbit losses establish a potential well that electrostatically confines the ions and preserves quasineutrality. As can be seen from the temperature profile evolution (Fig. 7), the well is established on a time scale of order ~5–10 ms. The ion temperature is only weakly affected by the density collapse.

During the unstable phase, the plasma rotates poloidallly with peak speed $\lesssim$2 km/s, the region closest to the central ring conductor being blueshifted (as indicated by the false color encoding of the contour plot). Zero flow velocity in this figure corresponds to a match between the phase of the plasma light interferogram and that from the laser calibration pulse. The apparent but fictitious flow speed bias of around 2000 m/s is equivalent to an instrumental phase mismatch $\delta\phi=(\delta v/c)\phi_0=10°$. This offset, which has no bearing on the measured relative phase offset between adjacent channels, corresponds to a frequency difference of 4 GHz between the laser source and the plasma emission line and is comparable with the laser intercavity mode spacing of ~1 GHz. The flow is consistent with bulk rotation of plasma associated with the predominant $m=1$ instability seen more clearly in Fig. 8. Given oscillation frequency $f_{\mathrm{mode}}=6.8$ kHz the associated rotation velocity of 2100 m/s (for rotation radius 0.05 m) is close to the observed value. The region of strong velocity shear in the edge region of the plasma may be associated with strong edge potential gradients observed in these discharges.[14]

Figure 8 shows a full resolution view of the camera projection data around the time of the collapse. The intensity shows a clear odd parity instability previously reconstructed using the FIC scanning interferometer.[15] Note the absence of associated ion temperature fluctuations and the clear even parity flow oscillation. The slow component of the flow profile has been removed in order to accentuate the oscillating part. This flow oscillation could be interpreted as a periodic displacement of the plasma center of rotation or an even parity plasma deformation made visible by the asymmetric intensity weighting of the Doppler shift.

Figure 9 shows data for an argon discharge exhibiting spontaneous transitions to states of higher particle and/or energy confinement. The line-integral electron density jumps by approximately 15% at times 18 ms and 40 ms into the discharge. As can be seen in the figure, the transitions are accompanied by comparable increases in the light emission intensity and associated discontinuities in the ion tempera-

Downloaded 20 Jun 2001 to 150.203.2.85. Redistribution subject to AIP license or copyright, see http://ojps.aip.org/rsio/rsicr.jsp

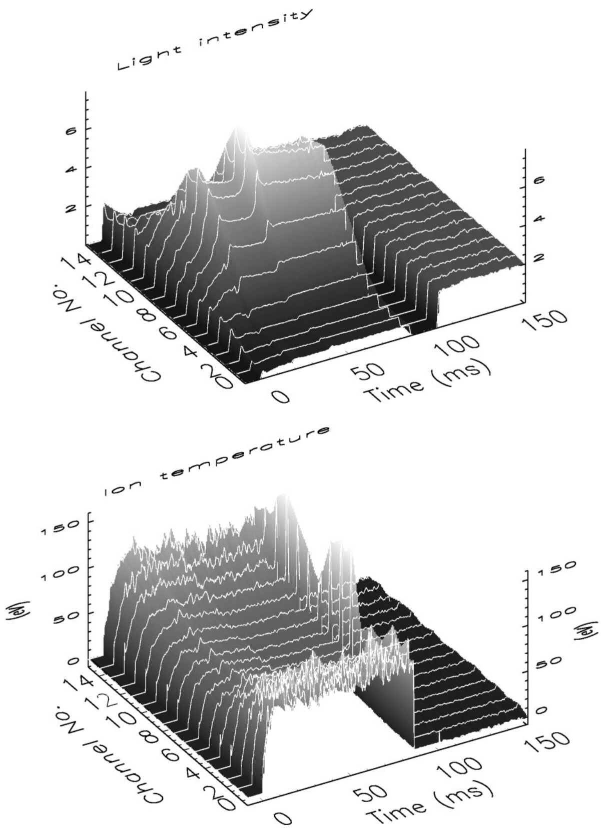

FIG. 9. Camera projection data for a discharge at higher field (0.22 T) showing multiple confinement transitions. Top: the light intensity (a laser calibration light pulse is admitted at time 100 ms). Bottom: the inferred intensity weighted ion temperature.

ture profile. These data, obtained using sixteen detector channels, illustrates the high spatial and temporal resolution (1 ms) that can be obtained using the camera. Note the approximately symmetry of the profiles. The greater ion temperature noise in the edge is due to the very low emission intensity in this region. The hollow ion temperature profile and the relaxation at the completion of the pulse are consistent features in these discharges.

B. ToMOSS

Uncertainties with interpretation of the flow data can be alleviated by viewing the plasma from many angles simultaneously. The ToMOSS spectroscopy experiment is designed to obtain detailed tomographic reconstructions of plasma flow fields and temperature distributions in the H-1 heliac.[7] A large diameter (~800 mm) rotatable stainless steel ring that encircles the plasma in a poloidal cross section is used for mounting five independent modules each containing 11 lens-coupled optical fibers for collecting plasma light along parallel chords separated by ~20 mm. Figure 10 shows the mounting ring, supporting frame, and the five sets of viewing chords superimposed on the plasma cross section. A photograph of one of the optical modules showing the collecting lenses is given in Fig. 11.

The optical fibers are wrapped around the edge of the wheel and are shielded from the plasma. The lenses can be rotated away from the plasma region when not in use. An

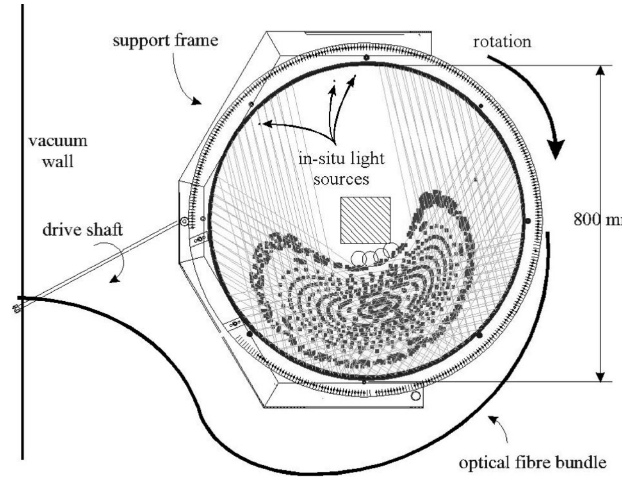

FIG. 10. Schematic drawing of ToMOSS optical ring and support structure showing the plasma region and viewing chords.

array of narrow (4 mm) fluorescent tubes are located in the viewing cross section (above the plasma region) for calibrating the relative channel sensitivities. The fibers exit the H-1 vacuum chamber via rubber O-ring seals and terminate at a patch panel. The rotatable ring, which has been recently installed, is driven by a stepper motor outside the vacuum vessel under CAMAC control. Light from the 55 channels will be fibre coupled to an imaging MOSS camera and the parallel signals acquired via CAMAC.

V. SPREAD-SPECTRUM METHODS—THE SOFT SPECTROMETER

A generalization of the MOSS spectrometer that utilizes a number of birefringent electro-optic plates mutually aligned at 45° and placed between crossed or parallel polarizers has been constructed and tested. The SOFT spectrometer allows simultaneous measurements of the coherence envelope of a narrow band spectral feature at a multiplicity of delays. As its name suggests, the information is now encoded across a series of harmonics of the common sinusoidal drive voltage applied to the electro-optic crystals.[8] The instrument is the coherence analog of a slit spectrometer equipped with an image plane detector array. The SOFT, however, uses a single fast detector, where the ''spectral'' pixels are the harmonic carriers in the temporal frequency domain.

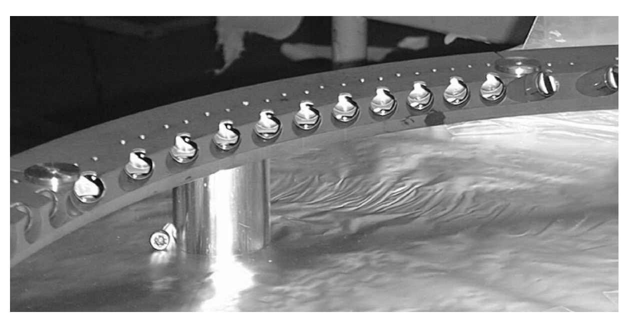

FIG. 11. Photograph of lens-coupled fiber module. The lenses are 15 mm in diameter. Five such modules are mounted on the carrier ring at intervals of 45°.

Downloaded 20 Jun 2001 to 150.203.2.85. Redistribution subject to AIP license or copyright, see http://ojps.aip.org/rsio/rsicr.jsp

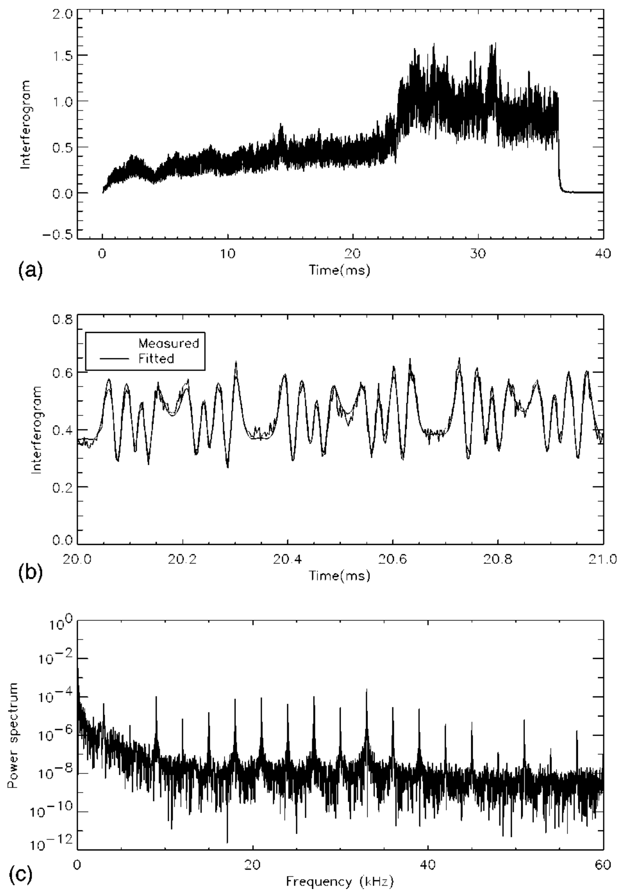

FIG. 12. SOFT data: (a) the measured interferogram, (b) expanded view showing measured and fitted signal, and (c) the power spectrum associated with (a).

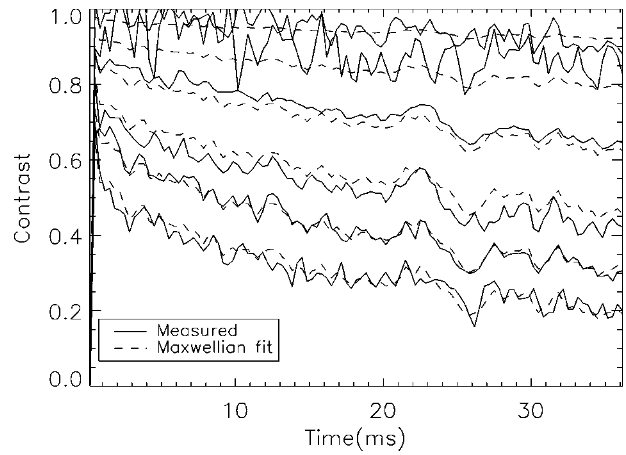

FIG. 13. (Solid curves) time evolution of the fringe visibility (contrast) for the interferogram shown in Fig. 12. The six curves correspond in top down order to successively larger delay offsets. (Dashed curves) the contrast that would be expected for the Maxwellian distribution that best fits the measurement set. Note the decreasing contrast with time as the plasma ion temperature rises to a maximum 20 eV.

We have used three crystals (thicknesses: 5, 20, and 40 mm) to generate six independent interferometers modulated about fixed delays $\phi_0=[3,5,7,9,11,13]\times 1000$ waves. Because the modulation indices ϕ_{1i} are in the same ratio as the delays ϕ_{0i}, the larger the delay, the greater the modulation depth and the higher in frequency are the generated harmonic carriers.

The interferogram can be processed numerically using a series of bandpass filters centered on the respective carriers and having a bandwidth determined by the plasma properties and the modulation frequency. Inverse fast Fourier transform recovers a set of time vectors which can be unwrapped to extract 12 independent pieces of information pertaining to the spectral line shape. Roughly speaking, the drive voltage should be sufficient to produce a modulation depth of at least $\pi/2$ radians for the interferometer having the least phase delay offset, to ensure data inversion with good condition number. The SOFT spectrometer is ideal for the study of nonthermal or complex spectra or for effectively extending the dynamic range of the MOSS spectrometer.

First measurements made with this system are presented here. Figure 12 shows the detailed interferogram and its reconstruction based on the computed contrasts, together with the calculated signal power spectrum which clearly shows the harmonic carriers. The unfolded, time-resolved contrasts at the six independent delays ϕ_0 are shown in Fig. 13. The system has been calibrated using an argon ion laser also tuned to 488 nm wavelength. While the overall agreement is good, there are some systematic discrepancies between the contrasts for the best fit Maxwellian and those observed. We tentatively attribute this to inaccuracies in the instrument calibration due to differences in the light input coupling for the laser and plasma. We plan to resolve these uncertainties in the near future.

VI. POLARIZATION SPECTROSCOPY

It is often the case that spectral lines are also split by magnetic or electric fields. The amount of splitting and the polarization orientation of the multiplet components convey information about the vector fields **B** or **E**. By modulating the polarization state of the multiplet, it is possible to vary the spectral content of the light. The change in the spectral shift or width is then sensed by the MOSS spectrometer as a variation of the interferogram phase or visibility. The phase and amplitude of these modulations give information about the orientation and magnitude of the originating field (electric or magnetic).

The applicability of a combined polarimeter and MOSS spectrometer for motional stark effect (MSE) measurements has been described elsewhere.[10] The primary advantages are higher light throughput and the elimination of narrowband interference filters for isolating the central σ cluster of lines. Here we summarize the basic measurement principle for MSE and indicate the suitability of the MOSS camera for such measurements.

MSE polarimetry is now a standard diagnostic for estimating magnetic field pitch angle in tokamaks using high power heating beams.[16,17] The MSE technique relies on the splitting of the high energy neutral beam Balmer α light into orthogonally polarized σ and π components as a result of the motion-induced strong electric field $\mathbf{E}=\mathbf{v}\times\mathbf{B}$ experienced in the rest frame of the neutral atoms. When viewed in a direction perpendicular to **E** the Stark split σ and π components

Downloaded 20 Jun 2001 to 150.203.2.85. Redistribution subject to AIP license or copyright, see http://ojps.aip.org/rsio/rsicr.jsp

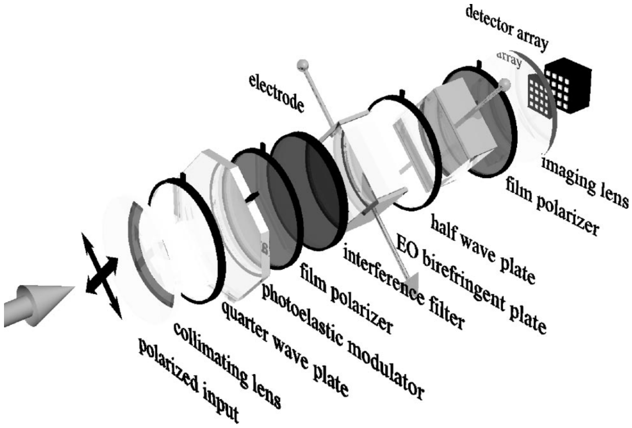

FIG. 14. Optical layout for the combined polarimeter/MOSS camera.

are polarized, respectively, perpendicular and parallel to the direction of **E**. When viewed along **E** the σ components are unpolarized and the π components have no intensity. The magnetic field pitch angle is usually estimated by isolating and measuring the polarization direction of the central cluster of σ lines.

We propose to filter the polarization of the multiplet using a polarimeter constructed of two birefringent phase plates (delays δ_1 and δ_2) having their fast axes mutually oriented at 45° followed by an analyzer oriented to transmit light polarized parallel to the fast axis of the first phase plate (the x direction). The final polarizing plate is superfluous when the polarimeter is used in combination with the MOSS camera (see Fig. 14).

For incident spectrum $e(\xi)$ The intensity of the light transmitted (or reflected) by the analyzer is related to the Stokes vector of the input radiation by [18]

$$P=\frac{e}{2}(1\pm\mathbf{s}\cdot\mathbf{p}),$$

$$\mathbf{s}=(\cos 2\psi\cos 2\chi,\sin 2\psi\sin 2\chi,\cos 2\chi), \tag{13}$$

$$\mathbf{p}=(\cos\delta_2,\sin\delta_2\sin\delta_1,\sin\delta_2\cos\delta_1),$$

where **s** is the Stokes vector, ψ is the tilt angle of the vibrational ellipse, and χ the ellipticity. If the phase plates are replaced by photoelastic modulators operating at frequencies Ω_1 and Ω_2 it is possible, using appropriate delay amplitudes and synchronous detection techniques, to measure simultaneously all the components of **s**.

Fixing the first phase plate delay $\delta_1=\pi/2$ (quarter wave plate) and sinusoidally modulating the second phase plate delay $\delta_2=\delta\sin\Omega_P t$ with modulation amplitude $\delta=\pi/2$ we obtain for the output intensity at the two polarimeter ports

$$2P_{\pm}(\xi)=e(\xi)[1\pm\zeta_P(\xi)\cos(2\psi-\delta\cos\Omega_P t)], \tag{14}$$

where $e=e_\sigma+e_\pi$ is the total intensity and $\zeta_P=(e_\sigma-e_\pi)/(e_\sigma+e_\pi)$ is the net polarization ''contrast.'' We have taken ψ as the orientation of the σ components and set $\chi=0$. Provided the difference $e_\sigma-e_\pi$ in component intensities is sufficiently great, the polarimeter signals will give the quadrature components $\sin(2\psi)$ and $\cos(2\psi)$ at Ω_P and $2\Omega_P$, respectively.

Since the integrated intensities for the σ and π components are comparable,[19] some spectral discrimination is required to increase the polarization contrast. The standard approach is to isolate the σ components using a narrowband interference filter. This is satisfactory provided the Stark splitting is sufficiently large for the π components to fall substantially outside the filter passband. It is also necessary that the splitting be large or comparable to the spectral broadening of the line due to the neutral beam divergence or range of viewing angles. Tilt-tuned narrowband interference filters are required for each observing position. The filters are lossy and make no use of the available π light. All these issues bear on the achievable signal-to-noise ratio which in turn limits the range of beam energies and magnetic field strengths for which MSE is useful.

The polarimeter transmits alternately the π and σ manifolds using polarization modulation techniques at frequency Ω_P. Since the spectral bandwidth of the π manifold is greater than for the central σ components, the MOSS spectrometer can enhance the signal modulation depth given an appropriate choice of time delay τ.

Because of its wide field-of-view a combined polarimeter/MOSS camera can be located close to the viewing port and the signals relayed by optical fiber to one or more detector arrays. Since the full multiplet is observed, only a relatively wideband interference filter is required to isolate the full energy emission spectrum. Given judicious choice of viewing geometry and filter alignment, such a wideband filter could be used for a number of viewing channels simultaneously. For the combined system, the light intensity at the final transmit polarizer port is given by

$$S=I_0/2[1+\zeta_I\zeta_{\mathrm{MSE}}\cos(\phi_0+(\pi/2)\cos\Omega_M t)],$$

$$\zeta_{\mathrm{MSE}}=[(\zeta_\sigma\cos^2\Psi+\zeta_\pi\sin^2\Psi)\cos\Phi], \tag{15}$$

$$\Psi=2\psi+\delta_2\cos\Omega_P t,$$

where Ω_P and Ω_M are the modulation frequencies for the polarimeter plate and the MOSS birefringent plate, respectively. Taking $\Omega_P<\Omega_M$, it is apparent that the ellipse orientation ψ is carried by the phase of the contrast modulation (at frequency Ω_P) impressed on the MOSS interferometer carrier signal (at Ω_M). The depth of this amplitude modulation $\zeta_\sigma-\zeta_\pi$ yields the magnetic field strength $|\mathbf{B}|$. Variations in beam energy will be registered as changes in the offset phase ϕ_0. For simplicity (though not necessity) the above analysis has assumed that the total intensities of the σ and π manifolds are comparable.[19]

ACKNOWLEDGMENTS

It is a pleasure to acknowledge technical assistance provided by J. Wach, M. Blacksell, and Rob Davies. Thanks are also due to Professor J. Harris for his ongoing support and to Dr. B. Blackwell for continuing smooth H-1 operations.

Downloaded 20 Jun 2001 to 150.203.2.85. Redistribution subject to AIP license or copyright, see http://ojps.aip.org/rsio/rsicr.jsp

[1] J. Howard, Rev. Sci. Instrum. **70**, 368 (1999).
[2] J. Howard, Appl. Opt. (submitted).
[3] J. Jacquinot, J. Opt. Soc. Am. **44**, 761 (1954).
[4] D. Steers, B. A. Patterson, W. Sibbett, and M. J. Padgett, Rev. Sci. Instrum. **68**, 30 (1997).
[5] S. Hamberger, B. Blackwell, L. Sharp, and D. Shenton, Fusion Technol. **17**, 123 (1990).
[6] C. Michael, J. Howard, and B. D. Blackwell, Rev. Sci. Instrum. (in press).
[7] F. Glass and J. Howard, Rev. Sci. Instrum. (these proceedings).
[8] J. Howard, J. Opt. Soc. Am. A (in preparation).
[9] R. J. Bell, *Introductory Fourier Transform Spectroscopy* (Academic, New York, 1972).
[10] J. Howard, Plasma Phys. Controlled Fusion **38**, 489 (1996).
[11] G. Warr, B. D. Blackwell, J. Wach, and J. Howard, Fusion Eng. Des. **34–35**, 387 (1997).
[12] W. Steel, *Interferometry* (Cambridge University Press, Cambridge, 1967).
[13] D. Miljak (private communication).
[14] M. Shats, D. L. Rudakov, R. W. Boswell, and G. G. Borg, Phys. Plasmas **4**, 3629 (1997).
[15] G. Warr, PhD. thesis, Research School of Physical Sciences and Engineering, Australian National University, Canberra 0200, Australia, 1998.
[16] F. M. Levinton *et al.*, Rev. Sci. Instrum. **61**, 2914 (1990).
[17] D. Wroblewski and L. L. Lao, Rev. Sci. Instrum. **63**, 5140 (1992).
[18] J. Howard, Rev. Sci. Instrum. **66**, 383 (1995).
[19] J. Xu *et al.*, Fusion Eng. Des. **34–35**, 293 (1997).

Downloaded 20 Jun 2001 to 150.203.2.85. Redistribution subject to AIP license or copyright, see http://ojps.aip.org/rsio/rsicr.jsp